Intelligent Maritime Networking With Edge Services and Computing Capability

Xin Su, *Senior Member, IEEE*, Leilei Meng, and Jun Huang, *Senior Member, IEEE*

***Abstract*—Maritime networks (MNs) typically cover tens to hundreds of kilometers, which can perform global oceanic observations via the support of maritime low-latency applications. However, current research on MNs with 5G related robust network optimization technologies, has not been progressed in line with the rapid development of terrestrial communication networks. To explore the oceanic informatics resources in the 5G or upcoming 6G eras, this work provides a method for intelligent maritime networking by conducting analysis, and investigation on maritime communication scenarios, probabilistic ship density, and MN connectivity. The edge-based MN services, and the edge computation capability based on a cognitive big data platform are thoroughly analyzed. The developed theory is extensively simulated, the real-world-trace based results further confirm the validity of the proposed method.**

***Index Terms*—Connectivity, edge computing, maritime network, SANET, URLLC.**

I. Introduction

MARITIME network (MN) is a networking paradigm that establishes multi-hop wireless communications to provide broadband service at sea. MNs can perform global oceanic observations and support low-latency applications by producing and processing oceanic cognitive big data. With the increasing demand on maritime ultra-reliable low latency communications (M-URLLC), one can envision that in the 5G or upcoming 6G (5/6G) era of MNs, using cloud computing via satellite relays will no longer meet the latency requirement of the maritime applications, such as navigation of unmanned vessels or unmanned underwater vehicles (UUV), collaborative scheduling of emergency disaster rescues, maritime real-time tracking and positioning, and low-latency observations and reactions in military services [1]–[6]. This is due to the fact that transitional satellite systems in MNs are commonly overloaded to process the maritime big data, leading to realize low delay maritime applications rarely, not alone they are under the harsh weather [1]. Considering the promising feature of edge computing compared with cloud computing, edge-computing-based intelligent maritime networking should be thoroughly investigated in order to overcome the aforementioned disadvantages from the satellite relay systems. Edge computing refers to infrastructure that enables data processing as close to the source as possible [7]–[9]. It allows for faster processing of data, reducing latency and improving customer experiences. For large-scale networks, such as MN, the need for rapid processing extends beyond customer satisfaction. Maritime networking can establish multi-hop networks to offer broadband services at ocean, gathering various kinds of maritime vessels [10], [11]. It has two distinguishing characteristics: highly affected by maneuver at sea-dynamic link quality and bandwidth constrained. Unlike land networking, maneuver at sea is affected by sea surface movement and wave occlusions, which can cause unstable environment with a high rate of link breakages caused by low link stability, as well as low and highly variable bandwidth.

While exciting progress has been made from both academia and industry, for example, 5G URLLC settings, defined by the International Telecommunication Union, mainly focus on the vehicle-to-vehicle (V2V), vehicle-to-infrastructure (V2I), and unmanned driven systems [12], [13]. Robust network optimization techniques, e.g. network function virtualization (NFV) [14], software-defined networking (SDN) [15], and edge/fog computing [16] for URLLC, have been well studied from the perspective of terrestrial networking to support low-latency applications [17]. Research on maritime communication and networking based on 5G technologies, however, has not progressed in line with the rapid development of terrestrial communication networks and is lagging behind. This can be evidenced by a recent survey on MNs that most of the existing studies aim at MNs' physical and data-link layers [1], [18], [19], leaving the service-based MNs network layer untouched. Therefore, more efficient maritime networking functions in terms of latency, reliability, data rate, and computing capability should be enhanced further by the state-of-the-art network layer architectures.

Note that, the research of MNs at the network layer from the perspective of M-URLLC should start from the maritime networking in terms of network probabilistic and connective models. By referring to the terrestrial networking research work, we find that the MNs typically features differing from terrestrial networks. More specifically, the following challenges of maritime networking must be dealt with:

- The MN usually covers approximately ten to hundreds of kilometers, the signal transmission delay should be considered as an important factor.

Manuscript received March 24, 2020; revised June 15, 2020; accepted August 2, 2020. Date of publication August 11, 2020; date of current version November 12, 2020. This work was supported in part by the National Natural Science Foundation of China under Grant 61801166 and in part by the Fundamental Research Funds for the Central Universities under Grant 2019B22214. The review of this article was coordinated by Dr. F. Tang. *(Corresponding author: Jun Huang.)*

Xin Su and Leilei Meng are with the College of IOT Engineering, Hohai University, Changzhou 213022, China (e-mail: leosu8622@163.com; 18360821591@163.com).

Jun Huang is with the School of Computer Science, Chongqing University of Posts, and Telecom, Chongqing 400065, China (e-mail: huangj@ieee.org).

Digital Object Identifier 10.1109/TVT.2020.3015751

- The MN has a different network topology from terrestrial networks because the terminal motion usually is not limited by the street layout.
- Terminal density at the offshore area usually is higher than it at an open-sea area, while the terminal speed is comparatively slow.
- The communication links in MNs are vulnerable to the environmental factors, such as harsh weather and water-waves.

The goal of this study is to establish a networking model for MNs under the umbrella of edge-computing, which can efficiently support various applications in 5/6G. The contributions of this work are summarized as follows.

- We devise an edge-computing-based MN system, in which the SDN and edge computing are employed to support the interoperability of heterogeneous MNs and to enable ultra-reliability, scalability, and low latency in MN, respectively. This system is dedicated to meet the rapid growth of marine vessels' demand for rapid computing and communication capabilities.
- We characterize communication scenarios in the offshore and open-sea area under practical conditions of curvy coastline and terminal motion trajectory consideration. The MN densities under the offshore and open-sea scenarios are formally modeled based on the spatial Poisson and random waypoint model (RWPM), respectively.
- Based on the established density models, we obtain the network connectives in the above scenarios by taking the maritime environmental factors into account. The MN connectivity is found affected by the variables of ship density, mobility, signal coverage, a distance of coast base station, water waves and so on, where the relations and effectiveness are modeled and analyzed by this study.
- We carry out extensive simulations to gain the insight into connection probabilities and to verify the effectiveness of the proposed models. We also present the analytical MN edge computing capability in Shanghai and Hong Kong offshore areas by tracking the cognitive big data platform of automatic identification system (AIS) [20]. We ultimately leverage a statistical means to acquire different ship information from AIS, such as the number of ships within an area, ship mobility statues and trajectories. According to that, we illustrate the maritime applications supported by edge services, and simulate the edge computing capacity along the seacoasts of cities of Hong Kong and Shanghai based on the AIS big data platform.

The remainder of this paper is organized as follows: Section II discusses the related work of the paper. Section III provides the details of the maritime networking in terms of system overview, communication scenario, and probabilistic densities, and Section IV builds up the maritime connectivity models under the offshore and open-sea environments, respectively. Section VI implements MN networking simulation experiments, and describes maritime edge services with edge-computing capability. Finally, the paper is concluded in Section VI. The terms and abbreviations are summarized in Table I.

TABLE I
TERMS AND ABBREVIATIONS

Abbreviation	Explanation
MN	Maritime network
M-URLLC	Maritime ultra-reliable low latency communications
UUV	Unmanned underwater vehicles
V2V	Vehicle-to-vehicle (V2V)
V2I	Vehicle-to-infrastructure
NFV	Network function virtualization
SDN	Software-defined networking
RWPM	Poisson and random way-point model
AIS	Automatic identification system
SANETs	Ship ad-hoc networks
VANETs	Vehicular ad-hoc networks
GPS	Global Positioning System
VHF	Very-high frequency
RTT	Radio transmission technology
IOCS	Intelligent ocean cloud server
SDNC	Software-defined networking controller
CU	Coastland unit
CUC	Coastland unit controller
SBS	Seacoast base station
S2S	Ship-to-ship
S2SBS	Ship-to-SBS

II. RELATED WORK

Since a limited number of existing studies have been focused on the maritime networking. We, in the following, summarize the research findings from the physical and data-link layers of ship ad-hoc networks (SANETs), and then compares the network connectivity models established for vehicular ad-hoc networks (VANETs). VANET is a particular case of a wireless multi-hop network, which has the constraint of fast topology changes due to the high node mobility [13].

A. Research on Ship Ad-hoc Networks

In general, the AIS consists of coastal base station facilities, ship-borne equipment, and satellite positioning systems. It is a digital navigation aid system [20] widely used in the Global Positioning System (GPS), in which the ship speed is tracked via very-high frequency (VHF) communication. With the increasing demand for 5G URLLC applications, such as maritime surveillance and underwater video sensing [6], [21], the AIS is unable to fulfill such service demands. It is evident that big data transmission not only causes higher network delays, but also increases the network operation costs. In addition, the AIS is vulnerable to environmental impacts, such as harsh weather. To address these problems, authors in [22] established a low-cost and high-rate maritime communication system in the VHF band. Thereafter the SANET was suggested, and research works have been conducted to enhance the performance of SANET in physical and data-link layers [1], [18], [19], [22]–[24]. Extensive studies on the SANET has proved that, as a counterpart to the VANET, it is expected to play a pivotal role in the 5/6G era of future MNs.

For studies in the physical layer of SANET, researchers set up a low-cost and high-data-rate architecture by constructing mesh and ad-hoc networks in the VHF band. Three different

TABLE II
VEHICULAR AD-HOC NETWORK CONNECTIVITY MODEL COMPARISONS

Ref.	Scenario	Model	Traffic Flow Model	Use of Basic Parameters					Special Parameters
				Vehicle			Infrastructure		
				Speed	Density	Converge	Separation	Coverage	
[22]	Urban	V2V	Street-Aware & Vehicles Following Model	Yes	Yes	Yes	No	No	Signal, Traffic rules
[23]	Urban	V2V, V2I	Realistic Data Stream	Yes	No	Yes	No	No	–
[24]	Highway	V2V	Poisson	No	Yes	Yes	Yes	No	Disconnected Link
[25]	Highway	V2V	Poisson	Yes	Yes	Yes	No	No	Outage Transmission Range
[26]	Highway	V2V, V2I	Poisson	No	Yes	Yes	Yes	Yes	–
[14]	Highway	V2V, V2I	Poisson	No	Yes	Yes	Yes	Yes	–
[27]	Highway	V2V, V2I	Poisson	Yes	Yes	Yes	No	No	–
[28]	Highway	V2V	Exponential	Yes	Yes	Yes	No	No	Safety Distance
[29]	Highway	V2V, V2I	Exponential	Yes	Yes	Yes	Yes	No	User Behavior

scenarios are considered, including ocean port, coast, and open-sea areas. The physical layer link reliability of the SANET architecture [19], [23], [24], i.e., the SANET radio transmission technology (RTT) is designed based on ITU-R 1842-1 standardization.

With respect to the SANET data-link layer, Ref. [1] employed the logical clock synchronization and effectively selected the synchronization time for the reference node by considering the propagation delay. In addition, the beacon collision was reduced through the adaptive timing synchronization process. Based on the simulation results, Ref. [1] redesigned the multi-hop frame structure to fulfill the requirements of SANET applications.

B. Research on Network Connectivity Models

The existing works on MNs have mainly focused on the physical and data link layers. Because few research works have done the maritime networking, in this paper, we mainly summarize the existing research works of VANET connectivity models in TABLE II, owing to the survey of VANET connectivity model that can help us for establishing a rational maritime networking work. The table lists comprehensive comparisons in terms of scenarios, communication modes, and node traffic flow, in the urban and highway scenarios. The key characteristics of vehicles self-organizing under the urban traffic model are subject to constraints of traffic lights, lane changes, and safety distance between the front and rear vehicles.

Authors in [25] consider the traffic signals and the different lengths of vehicles on the road and analyze the network connectivity for vehicles waiting at different intersections with safe distances. To further enhance the computation capability, distributed data fusion and convergence can be achieved via vehicular fog computing, as proposed in [26], where the variables affecting the capacity of the mobile cloud, such as the number of vehicles parked, dwell time mode, and the process of entering and leaving networks, are analyzed.

For highway traffic models, the vehicle's random arrival rate is observed to follow the Poisson process, as described in Based on prior conditions, Kwon *et al.* [27] established a point-line model, in which the geometric probability analysis was performed to derive the relationship between the connectivity and capacity of networks and ultimately obtain the total number of connections with the number of vehicles. To upgrade the assumption of constant mobility stated in [27], and authors in [28] modeled the vehicular mobility with a generalized stationary traversal stochastic process.

As the communication efficiency in an infrastructure-based VANET can be improved by introducing a vehicle-onboard relay network infrastructure, in [29], the communication for single-hop (direct access) and dual-hop (through relay) between the vehicle and infrastructure was considered, access and connectivity probability performances were depicted, and approximate equations are derived. In [17], the connectivity performance of the vehicle-onboard relay network based on infrastructure is analyzed. The connection probability of uplink and downlink is derived based on varied coverages and capacities of roadside units and vehicles.

In [30]–[32], research work on the varied vehicle equipment and driving safety were conducted, and the difference in network equipment was also considered. In the analysis, the transmission range of the vehicle is no longer a unified standard, but several variable parameters. The simulation result shows that appropriate device differentiation improves network connectivity. The safety issues of road driving and vehicle activity are also analyzed and discussed in [31] and [32], respectively. The analysis shows that driving safety distance and vehicle activity affect network connectivity, which provides a theoretical basis for future networks on VANET deployment.

In summary, the existing works on MNs have mainly focused on the physical and data link layers, in which the research findings help us to distinguish the major challenges different from terrestrial networks. To fully explore the maritime informatics resources, the investigation on the MN network layer is critical to enclose numerous robust network optimization techniques, such as NFV, SDN, and edge/fog computing, which are effective means for supporting M-URLLC. The existing works on terrestrial networking methods can guide us efficiently to build a correct and practical maritime networking model. This is the initial phase of future study to accomplish the smart MNs in the 5/6G era.

III. INTELLIGENT MARITIME NETWORKING

The existing studies have performed some in-depth research on the physical and data-link layers of SANET, and these research findings exhibit a solid theoretical basis for supporting maritime communications as well as effectively implementing integrated maritime services. In the 5/6G era of MNs, the application demands have increased significantly, e.g., low-latency

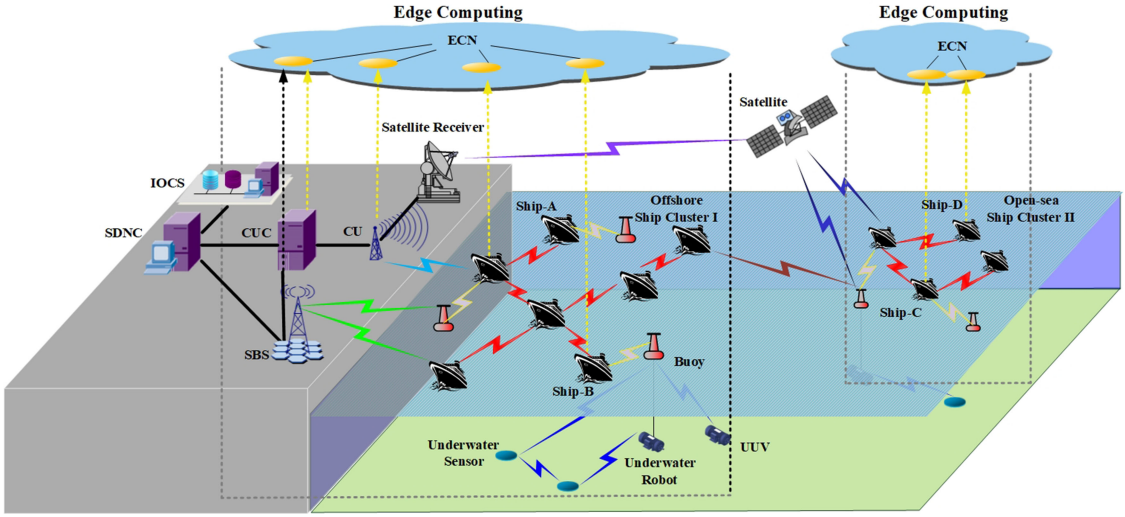

Fig. 1. Proposed infrastructure of edge computing-based MN.

observation and monitoring have become prominent, and thus requests to upgrade the MN have increased significantly. This study aims to fulfill the service requirements by increasing the network layer performances, where MN is divided into offshore and open-sea scenarios and the respective network connectivity probabilities are derived.

A. System Overview

In this study, a general MN infrastructure based on edge computing is proposed as shown in Fig. 1. In Fig. 1, intelligent ocean cloud server (IOCS) hosts virtual machines running on a service-driven platform to provide centralized data processing capabilities. The software-defined networking controller (SDNC) provides the networked intelligence of MNs to manage communications. It is a pivotal virtualization component that supports the platform and enables services at the edge of MN to obtain a set of processing capabilities closer to and faster for the users. The coastland unit (CU) is an access point located along the coastline for offshore ships or buoys. The coastland unit controller (CUC) is controlled by the SDNC. It acts as the head node for many CUs and connects to a CUC via broadband connections before accessing the SDNC. The seacoast base station (SBS) acts as a local server rather than as a voice and data conveying unit, and it is more sophisticated than the CUC. It is controlled by the SDNC, while delivering edge services. The ship and buoy nodes demonstrate sensing and communicating abilities and are capable of computing by acting as edge units. The underwater robot, sensor, and UUV are nodes with sensing, communicating, and limited computing abilities. Without the loss of generality, the satellite system is used as a backup communication resource to cover large distances among certain nodes in the open-sea area.

In the offshore area, ship navigation is not restricted by traffic signals, and ships parked and moving slowly can connect to each other to effectively act as a data fusion or a computing set. In the open-sea area, understanding the ship moving characteristics is necessary, as establishing stable and reliable base stations is impossible. Ships usually establish an ad-hoc manner network through interconnections and access core network through the satellite relay system. The interconnection of ships can also be used as mobile infrastructure, and the average length of the network connection duration needs to be estimated accurately.

B. Maritime Communication Scenario

The maritime communication system mainly comprises ships and SBSs, in which information interaction is achieved through ship-to-ship (S2S) and ship-to-SBS (S2SBS) communications. The SBS coverage is crucial to achieving a high network reliability in S2SBS communication. In case of S2S communication, the information exchanges between the ships need to guarantee adequate signal coverage by considering factors, such as ship arrival rate, speed, density, and the maximum number of transmission hops. Numerous ships in the offshore area mainly concentrate on major ports that can function together to accomplish large computing tasks and achieve efficient maritime edge computing capability. Fulfilling several computational demands is challenging because of the limited computing resources in a single ship. Therefore, a maritime edge computing architecture can be constructed to effectively utilize the ship computing nodes to form a powerful computing set and then rationally allocate the computing resources. In the open-sea area far from the seacoast, the ships cannot directly connect with SBS, and the S2S connections generally work in an ad-hoc manner. One or more relay nodes need to connect to a terrestrial core network to complete the relay task. In self-organizing, it is necessary to understand the rule of ship movement to reliably establish a network model and analyze the factors affecting connectivity. The crucial factors include ship speed, ship transmission range, and arrival rate.

C. Probabilistic Ship Density in Offshore Area

TABLE III lists all the parameters used in the rest of the paper with their notations. Fig. 2 illustrates an offshore communication scenario, where SBS_1 and SBS_2 are located along the coastline

TABLE III
THE PARAMETERS USED IN THE PAPER WITH THEIR NOTATIONS

Notation	Definition	Notation	Definition
$\tilde{L}$	Length of the sea coast	ϑ	Distance from any point in $B_r\,(d)$ to the center
L	Projection distance of $\tilde{L}$	T_c	Average time of the MN connection
R	SBS signal coverage	T_d	Average time of the MN disconnection
r	Ship transmission range	R_M	MN connection ratio
ρ	Poisson density of ship arrival rate	$\overline{T}_d$	Average MN disconnection time of a ship
μ	Ship average speed	$\hat{T}_d$	Average MN disconnection duration
σ^2	Gaussian variance of ship speed	$j(d)$	Probability of a ship demonstrating a distance d from the RWPM center
V	Probability density of ship speed	$\overline{T}_c$	Average MN connection duration
λ_0	Ship arrival rate	α, β, γ	Angles illustrated in Fig.2
$g_s(x)$	Probability of having a direct connection between two ships	p_f	Probability of a ship within r_1
$g_b(x)$	Probability of ship directly connected to SBS	p_r	Receive power of the destination ship
V_{min}	Minimum ship speed	p_l	Path loss index
V_{max}	Maximum ship speed	d_t	Reference distance
$\mathcal{A}$	Area of RWPM	p_t	Ship transmission power at d_t
$f(d)$	Probability of ship appearance rate at any point of $\mathcal{A}$	N_0	Additive Gaussian noise
d	Distance from the destination to the center point of $\mathcal{A}$	p_{th}	Certain threshold power
D	Destination or location in $\mathcal{A}$	σ_0	Variance of additive noise
ϕ	Direction toward the boundary of $\mathcal{A}$	κ	Propagation constant of electromagnetic waves
$\mathcal{A}\odot$	Center point of $\mathcal{A}$	f_ω	Signal frequency
$a_1(D,\phi)$	Distance from $D(D \in \mathcal{A})$ to the boundary of $\mathcal{A}$	ε	Dielectric constant of seawater
a_2	Distance to the boundary in the opposite direction	ε_0	Dielectric constant in vacuum
dA	A small region at point D	c	Speed of light
U_1, U_2	Destination connected on the path	ε_r	Relative dielectric constant
ℓ	Path length between U_1 and U_2	$\tilde{\mu}$	Magnetic permeability
$\ell \cap dA$	Path length within the interval dA	$\tilde{\mu}_0$	Magnetic permeability in vacuum
$\bar{\ell}$	Average length of the path ℓ	$\tilde{\mu}_r$	Relative magnetic permeability of the non-magnetic medium
$\mathcal{A}_j$	Subset of $\mathcal{A}$	τ	Electrical conductivity of seawater
$\lambda(\mathcal{A}_j)$	Average arrival rate at subset $\mathcal{A}_j$	$\tilde{\alpha}$	Real parts of the signal influenced by seawater
$\theta(d)$	Tangent line direction at point D	$\tilde{\beta}$	Imaginary parts of the signal influenced by seawater
N_{mob}	Number of moving ships	$\hat{r}$	Radius of the outer insulation shell
$\hat{P}$	Relationship between multi-hop connectivity and ship density	G_t, G_r	Transceiver gains
$S(x,r)$	Intersection of pair-ship communication ranges	δ	Water-wave period
$P_{2-hop}(x)$	Probability of ship communicating through two hops	λ_{wave}	Length of water-wave
k	The hop number	ζ	Initial phase of water-wave
$g(x)$	Probability of no ship directly connected to the destination	H	Maximum height of water-wave
$P_{k-hop}(x)$	k-hop relay probability with successful communication	$\angle\phi$	Inclination of the bow
P_s	Probability of a single ship accessing the SBS	$\angle\xi$	Inclination of the stern
P_a	Probability of ships near SBS accessing a single ship	L_{ship}	Length of the ship
$P_1(x)$	probability of Ship-B connecting directly to SBS	A	Coordinates of the ship
$P_2(x)$	Probability of ship directly connected to at least one ship unit	B	Antenna installation point
$P_s(x)$	Probability of a ship out of SBS connected to SBS_1 or SBS_2	h	Antenna height
$P_a(x)$	Probability of ships connected to SBS_1 or SBS_2 via multi-hop	$\vec{a}$	Direction vector of the communication antenna
$Q_{\hat{k}}\,(d,r)$	Probability of a ship connected to at least $\hat{k}$ adjacent ships	E	Vertex coordinates of the ship
$\hat{k}$	Number of ships connected to a mobile ship	E'	Vertex coordinates of the adjacent ship
$B_r\,(d)$	Area of ship signal coverage	m	Index of the water-wave

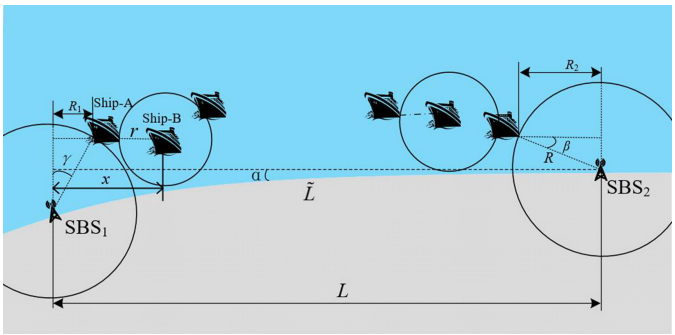

Fig. 2. Offshore communication scenario.

with a distance $\widetilde{L}$ (where L represents the projection distance). The SBS signal coverage is denoted as R, and the ship transmission range is r ($R > r$). In Fig. 2, Ship-B needs to communicate with SBS_1 through the Ship-A relay. If a ship is far from SBS, multiple relays are requested that inevitably increases the packet loss rate and reduces the network reliability. Therefore, we need to rationally build SBS_S by considering the best positions that can support the minimum number of relay connections to ensure network reliability.

It is assumed that the ship arrival rate is subject to spatial Poisson distribution with a density of ρ. Within length L, the number of ships follows the Poisson stochastic process with an average value of ρL. The probability distribution function of N ships within length L is defined as follows:

$$f(N,L) = \frac{(\rho L)^N e^{-\rho L}}{N!}. \tag{1}$$

By considering the ship mobility and setting the ship average speed as μ with a Gaussian variance σ^2, the probability density of the ship speed (denoted as V) can be expressed as follows:

$$f(V) = \frac{1}{\sigma\sqrt{2\pi}} \exp\left(-\frac{(v-\mu)^2}{2\sigma^2}\right). \tag{2}$$

According to 3σ criterion, the probability of normal distribution of a non-negative ship speed in the range of $[\mu - 3\sigma, \mu + 3\sigma]$ can attain 99.7%. Therefore, the ship speed is reasonably set to a random value within the range of $[V_{min} = \mu - 3\sigma, V_{max} =$

$\mu + 3\sigma]$. By applying the truncated Gaussian function deformation in Equation (2), we obtain

$$\widetilde{f}(V) = \frac{f(V)}{\int_{V_{min}}^{V_{max}} f(s)ds} = \frac{f(V)}{\int_{V_{\min}}^{V_{\max}} \frac{1}{\sigma\sqrt{2\pi}} \exp\left(-\frac{(s-\mu)^2}{2\sigma^2}\right) ds}. \quad (3)$$

By using Equation (4) to represent the truncated Gaussian function, a simplified deformation can be obtained as defined in Equation (5).

$$erf(x) = \frac{2}{\sqrt{\pi}} \int_0^x e^{-\eta^2} d\eta, \quad (4)$$

$$\tilde{f}(V) = \frac{2f(V)}{erf\left(\frac{V_{\max}-\mu}{\sigma\sqrt{2}}\right) - erf\left(\frac{V_{\min}-\mu}{\sigma\sqrt{2}}\right)}. \quad (5)$$

As $\widetilde{V} \sim \widetilde{f}(V)$, the velocity distribution of mobile ships and their density (ship/nautical-mile) can be formalized as follows:

$$\rho_{mob} = \lambda_0 \int_{V_{\min}}^{V_{\max}} \frac{1}{V} d\widetilde{F}(V) = \lambda_0 \mathrm{E}\left[\frac{1}{\widetilde{V}}\right]. \quad (6)$$

where λ_0 denotes the ship arrival rate. The number of ships between adjacent base stations can be obtained by combining the density expressions as follows:

$$f(N, L) = \frac{(\rho_{mob} L)^N \cdot e^{-\rho_{mob} L}}{N!}. \quad (7)$$

Let $g_s(x)$ and $g_b(x)$ represent the probability of having a direct connection between two ships and that of a ship being directly connected to SBS, respectively. If the connections are independent of each other, we obtain $g_s(x) > g_s(x)$. This is because, the transmission power of SBS is usually greater than the one offered by a ship even with an exhibited advanced transceiver system.

D. Probabilistic Ship Density in Open-Sea Area

The ships in the open-sea area are connected in an ad-hoc manner to form a small-scale data exchange system. Exploring the mobile characteristics of ships is important, as the connectivity probability with average network connections should be determined accurately. In this work, the RWPM is extended to describe the open-sea model, because it can respond well to the MN characteristics and is easy to implement. In this study, we mainly consider the connectivity for any ship-k and the average time of the MN connection.

The RWPM defines that the node randomly arriving rate at destination; the speed of the moving process before arrival at the destination is stable with the velocity fall ranging from $[V_{min}, V_{max}]$, and the random staying time after reaching the destination. A trajectory of the node motion of RWPM is shown in Fig. 3. Let $\mathcal{A}$ represent the area of RWPM, as illustrated in Fig. 3, where the nodes are assumed to individually move in an independent manner. To study the connection probability among ships, it is necessary to deduce the probability of ship appearance rate $f(d)$ (a ship exists rate at a unit area) at any point $\mathcal{A}$, where

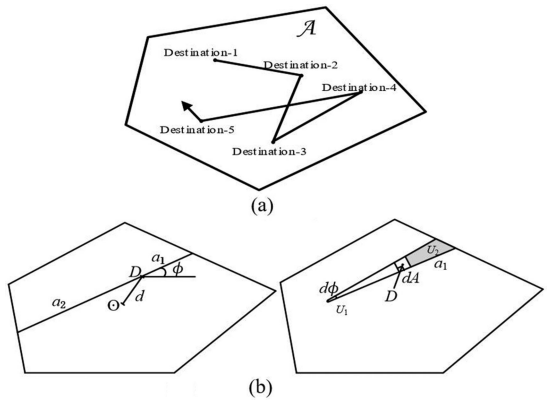

Fig. 3. Illustration of random way-point model (RWPM). (a) A node trajectory of RWPM. (b) Unit area of RWPM.

d represents the distance from the destination or location D to the center point $\mathcal{A}\bigodot$ of $\mathcal{A}$, as shown in Fig. 3.

To extend the RWPM based on Fig. 3 according to the open-sea communication characteristics, we define

$$h(d) = \frac{a_1 a_2 (a_1 + a_2)}{2}, \quad (8)$$

where $a_1(D, \phi)$ represents the distance from $D(D \in \mathcal{A})$ to the boundary of $\mathcal{A}$ in the direction ϕ, and a_2 represents the distance to the boundary in the opposite direction. Considering a small region dA at point D, it is observed that U_1 and U_2 are two destinations connected on the path. Assuming U_2 is in the shaded area, the path of U_1 to U_2 intersects with area dA, the path length between U_1 and U_2 is represented by $\ell = \|\overline{U_1 U_2}\|$, and $\ell \cap dA$ represents the length of the path within the interval dA. Thus, $f(d)$ can be expressed as

$$f(d) = \frac{\mathrm{E}[\ell \cap dA]}{\mathrm{E}[\ell]\, dA}. \quad (9)$$

The following can be obtained by the integral transformation of Equation (9):

$$f(d) = \frac{1}{\mathrm{E}[\ell]\, \mathrm{A}^2} \int_0^{2\pi} d\phi \int_0^{a_2} \left(da_1 + \frac{1}{2} a_1^2\right) dd. \quad (10)$$

According to the radial integration method, we obtain

$$f(d) = \frac{1}{\mathrm{E}[\ell]\, \mathrm{A}^2} \int_0^{2\pi} \frac{1}{2} a_1 a_2 (a_1 + a_2)\, d\phi. \quad (11)$$

By simplifying this equation, we obtain

$$f(d) = \frac{\int_0^{2\pi} h(d, \phi)\, d\phi}{C} = \frac{h(d)}{C}, \quad (12)$$

where $C = \overline{\ell}\mathcal{A}^2$, $h(d) = \int_0^{\pi} a_1 a_2 (a_1 + a_2) d\phi$, and $\overline{\ell}$ represents the average length of path. The average arrival rate at subset $\mathcal{A}_j \subset \mathcal{A}$ thus can be expressed as

$$\lambda(\mathrm{A}_j) = \int_{\partial \mathrm{A}_j} \lambda(d, \theta(d))\, dd, \quad (13)$$

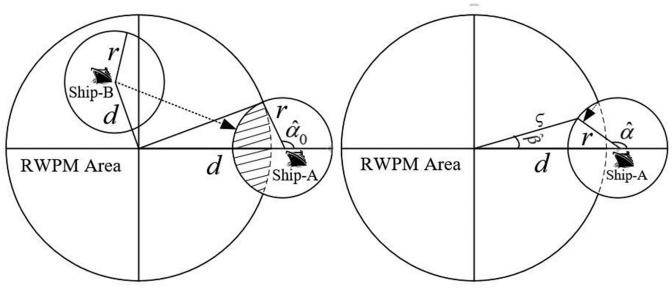

Fig. 4. Open-sea communication scenario.

where $\theta(d)$ is the tangent line direction at point D. Then

$$\lambda\left(d,\theta\right)=\frac{\int_0^{\pi}\sin\phi\cdot h\left(d,\theta+\phi\right)d\phi}{C\cdot \mathrm{E}\left(1/v\right)}. \tag{14}$$

Considering $\mathcal{A}$ as a unit circle, a_1 and a_2 can be expressed as

$$\begin{aligned} a_1(d,\phi)&=\sqrt{1-d^2\cos^2\phi}-d\sin\phi,\\ a_2(d,\phi)&=\sqrt{1-d^2\cos^2\phi}+d\sin\phi. \end{aligned} \tag{15}$$

As $a_1a_2=1-d^2$ and $a_1+a_2=2\sqrt{1-d^2\cos^2\phi}$, Equation (12) can be further simplified as follows:

$$f(d)=\frac{2\left(1-d^2\right)\int_0^{\pi}\sqrt{1-d^2\cos\phi}d\phi}{C}. \tag{16}$$

Assuming that a neighbor Ship-A is approaching the RWPM area, as illustrated by Fig. 4, the average ship arrival rate (for example, the probability of Ship-B arriving in the shaded area in Fig. 4 to connect to Ship-A) $\lambda(d,r)$ can be defined as follows:

$$\begin{aligned} \lambda\left(d,r\right)=\frac{45/64}{\pi\mathrm{E}\left(1/v\right)}\int_{\alpha_0}^{\pi}d\hat{\alpha}\cdot d\left(1-\varsigma^2\right)\int_0^{\pi}d\phi\\ \cdot\sin\phi\sqrt{1-\varsigma^2\cos^2\left(\phi+\hat{\alpha}-\hat{\beta}\right)}, \end{aligned} \tag{17}$$

where

$$\varsigma^2=d^2+2rd\cos\hat{\alpha}+r^2, \tag{18}$$

$$\hat{\beta}=\arctan(d+r\cos\hat{\alpha},r\sin\hat{\alpha}), \tag{19}$$

and

$$\hat{\alpha}_0=\begin{cases}0, & \text{when } r+d<1,\\ \arccos\frac{1-r^2-d^2}{2rd}, & \text{when } d-r<1\le r+d,\\ \pi, & \text{others.}\end{cases} \tag{20}$$

If the ship appears at the area center, we obtain $d=0,\varsigma=r,\hat{\alpha}_0=0$, and $\hat{\alpha}=\hat{\beta}$. Then Equation (17) can be expressed as

$$\lambda(r)=\frac{\left(45r\left(1-r^2\right)\right)\int_0^{\pi}\sin\phi\cdot\sqrt{1-r^2\cos^2\phi}d\phi}{64\mathrm{E}[1/V]}. \tag{21}$$

IV. Maritime Networking Connectivity

A. Offshore Connectivity in MN

1) Connectivity Among Ships: For the maritime single channel model, if the number of moving ships (N_{mob}) follows the spatial Poisson distribution, and the distance between adjacent ships follows the exponential distribution, the relationship between multi-hop connectivity and ship density is defined as follows:

$$\hat{P}=\prod_{i=1}^{N_{mob}-1}P\left(x_i\le r\right)=\left(1-e^{-\rho_{mob}r}\right)^{N_{mob}-1}, \tag{22}$$

where x represents the distance between the ships. Under the maritime multi-channel model, the intersection of pair-ship communication ranges can be defined as $S(x,r)$. If at least one ship in $S(x,r)$ performs as a relay node, the effective communication of the pair-ship can be guaranteed. The probability of at least one ship existing in $S(x,r)$ is given as

$$1-P(N=0,S(x,r))=1-e^{-\lambda'}=e^{-\rho_{mob}S(x,r)}. \tag{23}$$

Moreover, the ship signal range r demonstrates the following relationship with adjacent distance x:

$$\begin{cases} S(x,r)\in\left(\pi r^2,2r^2\arccos(\frac{x}{2r})-x\sqrt{r^2-\frac{x^2}{4}}\right), \\ \qquad\qquad\qquad\qquad \text{when } 0<x<r\\ S(x,r)=2r^2\arccos(\frac{x}{2r})-x\sqrt{r^2-\frac{x^2}{4}}, \\ \qquad\qquad\qquad\qquad \text{when } r<x<2r\\ S(x,r)=0, \qquad\qquad \text{others.}\end{cases} \tag{24}$$

When a pair of ships communicates with each other via two hops, the connection probability is defined as $P_{2-hop}(x)=1-e^{-\rho_{mob}S(x,r)}$. Typically, as the hop number k is higher than two, we need to determine the intersecting area $S(x,r)$. Based on Equation (23), the probability of realizing k-hop relay is defined as

$$1-g(x)=1-exp\left(-\int_{x-r}^{x+r}2P_{k-1}(x)\rho_{mob}r\theta dr\right), \tag{25}$$

where $g(x)$ is the probability of having no ship being directly connected to the destination. Therefore, the k-hop relay probability with successful communication is defined as

$$\begin{aligned} P_{k-hop}(x)=&\left(1-\sum_{i=1}^{k-1}P_i\left(x\right)\right)\\ &\left(1-\exp\left(-\int_{x-r}^{x+r}2P_{k-1}\left(r\right)\cdot\rho_{mob}\cdot r\cdot\theta dr\right)\right). \end{aligned} \tag{26}$$

2) Connectivity Between the Ship and SBS: We analyze the probability P_s of a single ship accessing the SBS and the probability P_a of all ships near SBS being able to access it. The former feeds back the satisfaction of user's experiences, while the latter reflects the service quality of MN. In addition, we need to consider the efficiency loss caused due to the multi-hop relay. In general, more hops result in higher interference and workload of extracting effective data. The two-hop relay usually can effectively extend the MN coverage to tens of kilometers to ensure efficient transmission.

According to Fig. 2, let the projection distance between Ship-B and SBS_1 be x, and the probability of Ship-B failing to connect to either SBS_1 or SBS_2 is $1-g_b(x)$ and $1-g_b(L-x)$,

respectively. Therefore, the probability of Ship-B connecting directly to SBS_1 or SBS_2 is defined as

$$P_1(x) = 1 - (1 - g_b(x))\,(1 - g_b\,(L - x))\,. \tag{27}$$

To derive the access probability P_s and P_a, we need two lemmas (refer to the appendix for the proofs) based on Fig. 2.

Lemma 1: A set of ships K in MN that can directly connect to SBS_1 or SBS_2 follow a non-uniform Poisson distribution with a density of $\rho P_1(x)$.

Lemma 2: Let $P_2(x)$ denote the probability of a ship (out of the SBS coverage) being directly connected to at least one unit of the ships within the coverage of SBS. Then we obtain

$$P_2(x) = 1 - \exp\left(-\int_0^L g_s(x)\cdot\rho_{mob}\cdot P_1(y)dy\right). \tag{28}$$

Let $P_s(x)$ indicate the probability of a ship out of SBS coverage accessing either SBS_1 or SBS_2 via multi-hop relay. Then we obtain

$$P_s(x) = 1 - (1 - P_1(x))\,(1 - P_2(x))\,. \tag{29}$$

Let $P_a(x)$ indicate the probability of all ships being connected to either SBS_1 or SBS_2 via multi-hop. Then we obtain

$$P_a(x) = \exp\left(-\int_0^L \rho_{mob}\cdot(1 - P_s(x))\,dx\right). \tag{30}$$

In addition, because usually $g_b(x) > g_s(x)$, they are expressed respectively as

$$g_b(x) = \begin{cases} 1, & x \le R \\ 0, & \text{otherwise} \end{cases} \quad g_s(x) = \begin{cases} 1, & x \le r \\ 0, & \text{otherwise,} \end{cases} \tag{31}$$

Combined with Equations (29) and (30), the access probabilities can be obtained in terms of six cases.

Case 1: When $0 < L \le 2R$ and $x \in [0, L]$, then $P_1(x) = 1, P_s = \frac{1}{L}\int_0^L P_s(x)dx = 1$, and $P_a(x) = 1$;

Case 2: When $2R < L \le 2R + r$ and $x \in (R, L - R)$, then $P_1(x) = 0$,

$$\begin{aligned} P_2(x) &= 1 - \exp\left(-\int_0^R g_s(x)\rho_{mob}dy - \int_{L-R}^L g_s(x)\rho_{mob}dy\right) \\ &= 1 - \exp\left(-\int_{x-r}^R \rho_{mob}dy - \int_{L-R}^{x+r}\rho_{mob}dy\right) \\ &= 1 - \exp\left(-\rho_{mob}\cdot(2R + 2r - L)\right) \end{aligned} \tag{32}$$

$$\begin{aligned} P_s(x) &= \frac{1}{L}\int_0^L P_s(x)dx = \frac{1}{L}\int_R^{L-R} 1 - (1 - P_2(x))dx \\ &= 1 - \frac{L - 2R}{L}\exp\left(-\rho_{mob}\,(2R + 2r - L)\right) \end{aligned} \tag{33}$$

$$P_a(x) = \exp\left(-(L - 2R)\cdot\rho_{mob}\cdot e^{-\rho_{mob}(2R+2r-L)}\right) \tag{34}$$

Case 3: When $2R < L \le 2R + r$ and $x \in (0, R) \cup (L - R, L)$, then $P_1(x) = P_s(x) = P_a(x) = 1$;

Case 4: When $2R + r < L \le 2R + 2r$ and $x \in (R, L - R)$, then

$$P_2(x) = 1 - \exp\left(-\int_0^R g_s(x)\rho_{mob}dy - \int_{L-R}^L g_s(x)\rho_{mob}dy\right) \tag{35}$$

$$\begin{aligned} P_s(x) &= \frac{1}{L}\int_0^L P_s(x)dx = \frac{1}{L}\int_R^{L-R} P_2(x)dx \\ &= 1 + \frac{2}{\rho_{mob}L}(e^{-\rho_{mob}r} - e^{-\rho_{mob}(2R+2r-L)}) \\ &\quad - \frac{2R + 2r - L}{L}e^{-\rho_{mob}(2R+2r-L)} \end{aligned} \tag{36}$$

$$p_a(x) = \frac{exp(-2(e^{-\rho_{mob}(2R+2r-L)} - e^{-\rho_{mob}r}))}{exp\left((2R + 2r - L)\cdot\rho_{mob}\cdot e^{-\rho_{mob}(2R+2r-L)}\right)} \tag{37}$$

Case 5: When $2R + r < L \le 2R + 2r$, and $x \in (0, R) \cup (L - R, L)$, then $P_1(x) = P_s(x) = P_a(x) = 1$;

Case 6: When $L > 2R + 2r$, then

$$\begin{aligned} P_s(x) &= \frac{1}{L}\int_0^L P_s(x)dx = \frac{1}{L}\int_R^{L-R} P_2(x)dx \\ &= \frac{2R + 2r}{L} + \frac{2(e^{-\rho_{mob}r} - 1)}{\rho_{mob}L} \end{aligned} \tag{38}$$

$$P_a(x) = \exp\left(-\left(2 - 2e^{-\rho_{mob}r} + \rho_{mob}\,(L - 2R - 2r)\right)\right) \tag{39}$$

B. Open-Sea Connectivity in MN

1) Connectivity Among Ships: For a ship moving in the open-sea area, let $Q_{\hat{k}}(d, r)$ represent the probability of the ship having at least $\hat{k}$ neighbors to connect with, and let $P(d, r)$ represent the probability of any neighbor ship being located within its coverage. Then we obtain

$$P(d, r) = \int_{\vartheta\in B_r(d)} f\,(|\vartheta|)\,d\mathrm{A}, \tag{40}$$

where $B_r(d)$ is the area of ship signal coverage, and ϑ represents the distance from any point in $B_r(d)$ to the center. Assuming that the ships are moving independently in $B_r(d)$ with the number following a binomial distribution, then the probability of a ship connecting to at least $\hat{k}$ adjacent ships is defined as follows:

$$Q_{\hat{k}}(d, r) = 1 - \sum_{i=0}^{\hat{k}-1}\binom{n-1}{i}P(d, r)^i(1 - P(d, r))^{n-i-1}. \tag{41}$$

By considering the RWPM, it can be further expressed as

$$\begin{aligned} Q_{\hat{k}}\,(d,r) = 2\pi\int_0^1 df(d) \\ \left(1 - \sum_{i=0}^{\hat{k}-1}\left(\binom{n-1}{i}p(d, r)^i(1 - p\,(d, r))^{n-1-i}\right)\right)dd. \end{aligned} \tag{42}$$

Therefore, the number of ships within $B_r(d)$ follows the Poisson stochastic process with its average value defined as

$$a(d) = (n-1)\pi r^2 \rho_{mob}. \tag{43}$$

Combining this with Equation (42), we obtain

$$Q_{\hat{k}}(d,r) = 1 - 2\pi \int_0^1 d\rho_{mob} \sum_{i=0}^{\hat{k}-1} \frac{a(d)^i}{i!} \cdot e^{-a(d)} dd, \tag{44}$$

where the probability of the number of ships in $B_r(d)$ being less than $\hat{k}$ is defined as $\sum_{i=0}^{\hat{k}-1} \frac{a(d)^i e^{-a(d)}}{i!}$.

2) Network Connection Duration: Let the random variables T_c and T_d represent the average time of the MN connection and disconnection, respectively. We can then define the MN connection ratio as

$$R_M = \frac{T_c}{T_c + T_d}. \tag{45}$$

Note that R_M is inversely proportional to r. The average MN disconnection time $\overline{T}_d$ of a ship can be defined based on Equation (9) as

$$\overline{T}_d \approx \frac{1}{(N-1)\cdot f(d)}. \tag{46}$$

Then the average MN disconnection duration is obtained by

$$\hat{T}_d = \int_d \overline{T}_d \cdot j(d) dd, \tag{47}$$

where $j(d)$ denotes the probability of a ship demonstrating a distance d from the RWPM center. Thus, finally we obtain average MN connection duration as follows:

$$\overline{T}_c \approx \frac{(Q_{n,1}(r))^n \overline{T}_d}{1 - (Q_{n,1}(r))^n}. \tag{48}$$

C. Analysis of Environmental Factors

Practically, the coastlines demonstrate angular changes, as shown in Fig. 2, where the length of the sea coast is represented by $\tilde{L}$ with an inclination angle of α and the vertical included angles of γ and β. Thus, we obtain $R_1 = \sqrt{R^2 - (S + R\cos\beta)^2}$ and $R_2 = R\cos\beta$, where $S = \sqrt{\tilde{L}^2 - L^2}$. The equation updates required to obtain the aforementioned P_s and P_a with $2R \to (R_1 + R_2)$ are redundant and therefore not provided here.

The differences among the maritime equipment lead to different energy consumptions associated with different signal coverage ranges. Let us assume that two ships demonstrate different signal coverages, i.e., the probability of a ship with coverage of r_1 is p_f, and that with coverage of r_2 is $1 - p_f$. Then we should extend some of the access probability cases.

For $Case-2$: Equations (32) and (33) are updated as follows:

$$p_2(x) = p_f\left(1 - e^{-\rho(2R+2r_1-L)}\right) + (1-p_f)\left(1 - e^{-\rho(2R+2r_2-L)}\right), \tag{49}$$

$$P_s = \frac{2R}{L} + \frac{L-2R}{L}\left(p_f(1 - e^{-\rho_{mob}(2R+2r_1-L)})\right) + \frac{L-2R}{L}\left((1-p_f)(1 - e^{-\rho_{mob}(2R+2r_2-L)})\right). \tag{50}$$

For Case-4: When $2R + r_2 < L \le 2R + 2r_1$ and $x \in (R, L-R)$, Equations (35) and (36) are updated as follows:

$$p_2(x) = \begin{cases} p_f\left(1 - e^{-\int_{x-r_1}^{R} \rho_{mob} dy}\right) & x \in (R,\ L-R-r_1] \\ (1-p_f)\left(1 - e^{-\int_{x-r_1}^{R} \rho_{mob} dy}\right) & x \in (R,\ L-R-r_1] \\ p_f\left(1 - e^{-\int_{L-R-r_1}^{R+r_1} \rho_{mob} dy}\right) & x \in (L-R-r_1,\ R+r_1] \\ (1-p_f)\left(1 - e^{-\int_{L-R-r_2}^{R+r_2} \rho_{mob} dy}\right) & x \in (L-R-r_2,\ R+r_2] \\ p_f\left(1 - e^{-\int_{L-R}^{x+r_1} \rho_{mob} dy}\right) & x \in [R+r_1,\ L-R) \\ (1-p_f)\left(1 - e^{-\int_{L-R}^{x+r_2} \rho_{mob} dy}\right) & x \in [R+r_2,\ L-R) \end{cases} \tag{51}$$

$$\begin{aligned} P_s = 1 &+ \frac{2p_f}{\rho_{mob} L}(e^{-\rho r_1} - e^{-\rho_{mob}(2R+2r_1-L)}) \\ &+ \frac{2(1-p_f)}{\rho_{mob} L}(e^{-\rho mobr_2} - e^{-\rho mob(2R+2r_2-L)}) \\ &- p_f \frac{2R+2r_1-L}{L} e^{-\rho_{mob}(2R+2r_1-L)} \\ &- (1-p_f)\frac{2R+2r_2-L}{L} e^{-\rho_{mob}(2R+2r_2-L)}. \end{aligned} \tag{52}$$

Meanwhile, when $2R + 2r_1 < L \le 2R + 2r_2$ and $x \in (R, L-R)$, Equations (35) and (36) are updated as follows:

$$p_2(x) = \begin{cases} p_f\left(1 - e^{-\int_{x-r_1}^{R} \rho_{mob} dy}\right) & x \in (R,\ R+r_1] \\ p_f\left(1 - e^{-\int_{L-R}^{x+r_1} \rho_{mob} dy}\right) & x \in [L-R-r,\ L-R) \\ (1-p_f)\left(1 - e^{-\int_{x-r_2}^{R} \rho_{mob} dy}\right) & x \in (R,\ L-R-r_2] \\ (1-p_f)\left(1 - e^{-\int_{L-R-r_2}^{R+r_2} \rho_{mob} dy}\right) & x \in (L-R-r_2,\ R+r_2] \\ (1-p_f)\left(1 - e^{-\int_{L-R}^{x+r_2} \rho_{mob} dy}\right) & x \in [R+r_2,\ L-R) \end{cases} \tag{53}$$

$$P_s = \frac{2R}{L} + \frac{1}{L}\left\{ \begin{array}{l} 2p_f r_1 + 2(1-p_f)(L-2R-r_2) + \frac{2p_f}{\rho_{mob}}(e^{-\rho r_1} - 1) \\ + \frac{2(1-p_f)}{\rho_{mob}}\left(e^{-\rho_{mob} r_2} - e^{-\rho_{mob}(2R+2r_2-L)}\right) \\ + (1-p_f)(2R+2r_2-L)\left(1 - e^{-\rho_{mob}(2R+2r_2-L)}\right) \end{array} \right\} \tag{54}$$

For $Case-6$, when $L > 2R + 2r_2$ and $x \in (R, L-R)$, $p_1(x) = 0$,

$$p_2(x) = \begin{cases} p_f\left(1 - e^{-\int_{x-r_1}^{R} \rho_{mob} dy}\right) & x \in (R,\ R+r_1] \\ (1-p_f)\left(1 - e^{-\int_{x-r_2}^{R} \rho_{mob} dy}\right) & x \in (R,\ R+r_2] \\ p_f\left(1 - e^{-\int_{L-R}^{x+r_1} \rho_{mob} dy}\right) & x \in [L-R-r_1,\ L-R) \\ (1-p_f)\left(1 - e^{-\int_{L-R}^{x+r_2} \rho_{mob} dy}\right) & x \in [L-R-r_2,\ L-R) \end{cases} \tag{55}$$

$$P_a = \frac{2R}{L} + \frac{1}{L}\left\{ \begin{matrix} 2p_f r_1 + 2(1-p_f) r_2 + \frac{2p_f}{\rho_{mob}}\left(e^{-\rho r_1} - 1\right) \\ + \frac{2\left(1-p_f\right)}{\rho_{mob}}\left(e^{-\rho r_2} - 1\right) \end{matrix} \right\}. \tag{56}$$

Moreover as $x \in (0, R) \cup (L-R, L)$, $p_1(x) = P_a = P_c = 1$.

The oceanic waves usually affect the communication links. To accurately explore the communication characteristics, we analyze the wave factors by considering long-term fading with lognormal shadow model as

$$p_r = p_t - 10 p_l \lg\left(\frac{x}{d_t}\right) + N_0, \tag{57}$$

where p_r is the received power of the destination ship, p_t is the ship transmission power at the reference distance d_t, p_l is the path loss index, and N_0 is the additive Gaussian noise. If the received power p_r is greater than a certain threshold power p_{th}, then communication can be established and a specific threshold can be set as follows:

$$p_{th}^{ship} = p_t - 10 P_l \lg\left(\frac{r}{d_t}\right), \tag{58}$$

$$p_{th}^{SBS} = p_t - 10 P_l \lg\left(\frac{R}{d_t}\right). \tag{59}$$

According to the lognormal model, we obtain

$$g_s(x) = \Pr\left(p_r \geq p_{th}^{ship}\right) = Q\left(\frac{10 p_l}{\sigma_0} \lg\left(\frac{x}{r}\right)\right), \tag{60}$$

where δ_0 is the variance of additive noise. The access probabilities P_s and P_a thus should be further updated. As the propagation of electromagnetic waves in seawater is completely different from that in the open-space, understanding the path loss p_l under the influence of waves is necessary.

For signal attenuation and phase change of electromagnetic waves in seawater, it is known that the propagation constant κ of electromagnetic waves is defined as

$$\kappa = \omega\sqrt{j\omega\tilde{\mu}\left(\tau + j\omega\varepsilon\right)} = \tilde{\alpha} + j\tilde{\beta}, \tag{61}$$

where $\omega = 2\pi f_w$, and f_w is the signal frequency. $\varepsilon = \varepsilon_0\varepsilon_r$ is the dielectric constant, where $\varepsilon_0 = 1/\sqrt{c^2\mu_0}$ is the dielectric constant in vacuum, and c is the speed of light. ε_r is the relative dielectric constant. Note that $\tilde{\mu} = \tilde{\mu}_0\tilde{\mu}_r$ is the magnetic permeability, and $\tilde{\mu}_0$ and $\tilde{\mu}_r$ represent the magnetic permeability in vacuum and the relative magnetic permeability of the non-magnetic medium, respectively. Finally, τ is the electrical conductivity of seawater.

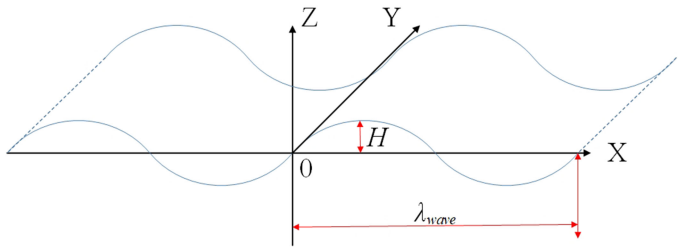

Fig. 5. Model of water-wave.

The real and imaginary parts of the signal influenced by seawater are thus expressed as follows:

$$\tilde{\alpha} = \sqrt{\frac{1}{2}\omega^2\tilde{\mu}\varepsilon}\sqrt{\sqrt{1 + \left(\frac{\tau}{\omega\varepsilon}\right)^2} - 1},$$

$$\tilde{\beta} = \sqrt{\frac{1}{2}\omega^2\tilde{\mu}\varepsilon}\sqrt{\sqrt{1 + \left(\frac{\tau}{\omega\varepsilon}\right)^2} + 1}. \tag{62}$$

As seawater is a good conductive medium, and the dielectric constant $\varepsilon = 81\varepsilon_0$, we obtain $\tilde{\alpha} = \tilde{\beta} \approx \sqrt{\pi f_w \tilde{\mu}\tau}$. The signal propagating through the seawater experiences an extended spatial loss and absorption of the seawater medium. Thus, we obtain

$$p_r = \frac{p_t G_t \left[4\pi(d_t + 2\hat{r})^{-2}\right] e^{-j2kd_t} G_r f_w^{-2}}{4\pi}, \tag{63}$$

where G_t and G_r denote the transceiver gains, and $\hat{r}$ is the radius of the outer insulation shell. In addition, if the gain of the transceiver is assumed to be one, the path loss can be simplified as

$$p_l = \frac{p_t}{pr} = \left(2\tilde{\beta} d_t\right)^2 e^{2\tilde{\alpha} d_t}. \tag{64}$$

As propagation distance is a major factor that influences the pass loss, obtaining the transmission distance of the signal being covered by seawater on the path is necessary.

As shown in Fig. 5, the water-wave can be mathematically represented as follows:

$$wave = H \sin\left[2\pi\left(\frac{t}{\delta} - \frac{x}{\lambda_{wave}}\right) + \zeta\right], \tag{65}$$

where δ is the wave period, λ_{wave} is the length, ζ is the initial phase, and H is the maximum height. Suppose the ship's contour is approximately described as an isosceles triangle tangent to a point on the surface of the water-wave, and points B, C, and D are used to represent the three vertices of the ship, as shown in Fig. 6. As the ship is affected by the waves, the inclination $\angle\phi$ of the bow and the inclination $\angle\xi$ of the stern are generated. Meanwhile, let point A (X_A, Y_A, Z_A), the midpoint of the CD line segment, indicate the coordinates of the ship and the tangent point between the ship and the sea wave. The length of the ship is set to $L_{ship} = \|\overrightarrow{AB}\|$. The communication antenna is installed at point B at the height of h. The direction vector of the communication antenna can be obtained by deriving the surface of the wave as follows:

$$\vec{a} = \left(\frac{1}{\lambda_{wave}} 2\pi H \cos\left[2\pi\left(\frac{\mathrm{t}}{\delta} - \frac{x}{\lambda_{wave}}\right) + \zeta\right], 0, 1\right). \tag{66}$$

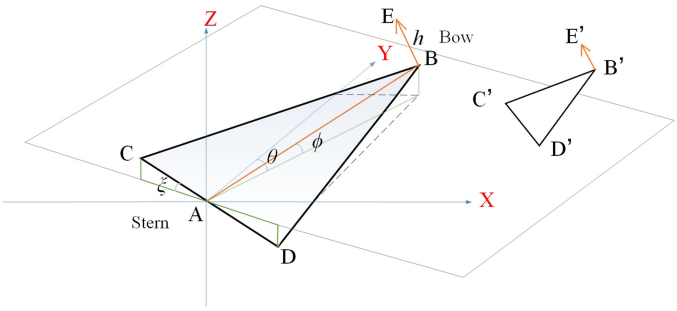

Fig. 6. Model of ship's relative position.

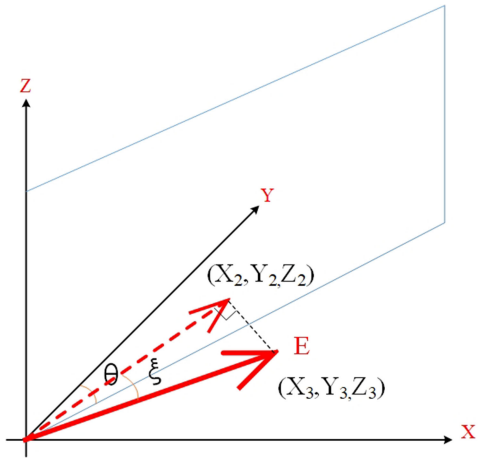

Fig. 7. Model of the relative position of antenna direction vector.

The coordinates of the antenna height at point E are obtained as follows:

$$\angle\xi = \arcsin\left[\frac{(\cot\theta, -1, 0)\cdot\vec{a}}{|\vec{a}|}\right]. \tag{67}$$

According to the direction vector model shown in Fig. 7, we obtain $\angle\phi = \arctan(\sqrt{X_{2'}+Y_{2'}}/Z_2)$ according to Equation (68).

$$\begin{cases} X_2X_3 + Y_2Y_3 + Z_2Z_3 = \left(X_3^2 + Y_3^2 + Z_3^2\right)\cos\xi \\ X_2^2 + Y_2^2 + Z_2^2 = X_3^2 + Y_3^2 + Z_3^2 \\ X_2 = Y_2\tan\theta \end{cases} \tag{68}$$

According to the geometric relationship, the coordinates of point B are defined as follows:

$$\begin{cases} X_B = X_A + L_{ship}\cos\phi\sin\theta \\ Y_B = Y_A + L_{ship}\cos\phi\cos\theta \\ \mathrm{Z_B} = \mathrm{Z_A} + L_{ship}\sin\phi \end{cases} \tag{69}$$

Then the coordinates of point E are defined as follows:

$$\begin{cases} X_E = X_B + h\sin\phi\sin\xi\sin\theta \\ Y_E = Y_B + h\sin\phi\sin\xi\cos\theta \\ \mathrm{Z_E} = \mathrm{Z_B} + h\cos\phi\cos\xi \end{cases} \tag{70}$$

Similarly, the vertex coordinates E′ of the adjacent ship (shown in Fig. 6) can be obtained. To deduce the equation of the line passing through points E and E′, the following transformation

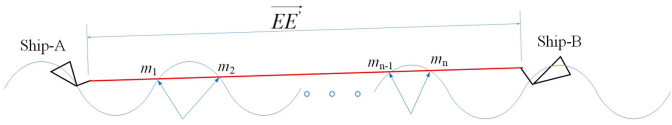

Fig. 8. Line of ships' antennae pass through the water waves.

TABLE IV
SIMULATION PARAMETERS

Parameter	Description	Value
Under Offshore Environment		
ρ_{mob}	Moving Ship Density	$0 \sim 0.1 ship/m$
r	Ship Signal Coverage	$300m, 500m$
R_1, R_2	SBS Coverages	$500m, 1km$
L	SBS Spacing	$0 \sim 8km$
μ	Mean of Ship Speed	$16, 24, 32knot$
σ	Standard Deviation of Ship Speed	$4, 7, 10knot$
Under Open-sea Environment		
r	Normalized Ship Communication Radius	$0 \sim 1$
k	Number of Connected Ships	$1, 2, 3$
N	Number of Ships	$20, 60, 100$

can be performed:

$$\frac{x - X_E}{X_E - X_E^{'}} = \frac{y - Y_E}{Y_E - Y_E^{'}} = \frac{z - Z_E}{Z_E - Z_E^{'}} = m$$

$$\begin{cases} x = m\left(X_E - X_E^{'}\right) + X_E \\ y = m\left(Y_E - Y_E^{'}\right) + Y_E \\ z = m\left(Z_E - Z_E^{'}\right) + Z_E \end{cases} \tag{71}$$

By substituting Equation (71) into Equation (65), we obtain

$$m\left(Z_E - Z_E^{'}\right) + Z_E = H\sin\left[2\pi\left(\frac{t}{\delta} - \frac{m\left(X_E - X_E^{'}\right) + X_E}{\lambda_{wave}}\right) + \zeta\right]. \tag{72}$$

Solving Equation (72) can provide a plurality of coordinate positions corresponding to m, which is the index of the water-wave, as shown in Fig. 8. The coordinate sequence corresponds to a set of intersections of ocean wave surfaces and straight lines passing through points E and E′. Determining whether the obtained intersection point is within the segment $\overrightarrow{EE'}$ is important. If it is not within the segment, it can be discarded. Using the intersection set of line and wave surface in $\overrightarrow{EE'}$ (m_1, m_2,... m_n), the length of the communication linear distance covered by the wave when two ships communicate is calculated as $d = \sum_{n=1}^{N} |\overrightarrow{m_{n-1}m_n}|$. From Equation (64), it is easy to deduce that the path loss index is affected not only by the dielectric properties, such as conductivity, permeability, and dielectric constant, but also by the frequency of the signal.

V. MN NETWORKING SIMULATION VERIFICATIONS

TABLE IV lists the simulation parameters settings, in which the moving density of ship defined by Equation (6) is varied from $0 \sim 0.1 ship/m$. We consider two ship signals with coverage $300\,m, 500\,m$, and the SBS signals with coverage $500\,m$ and

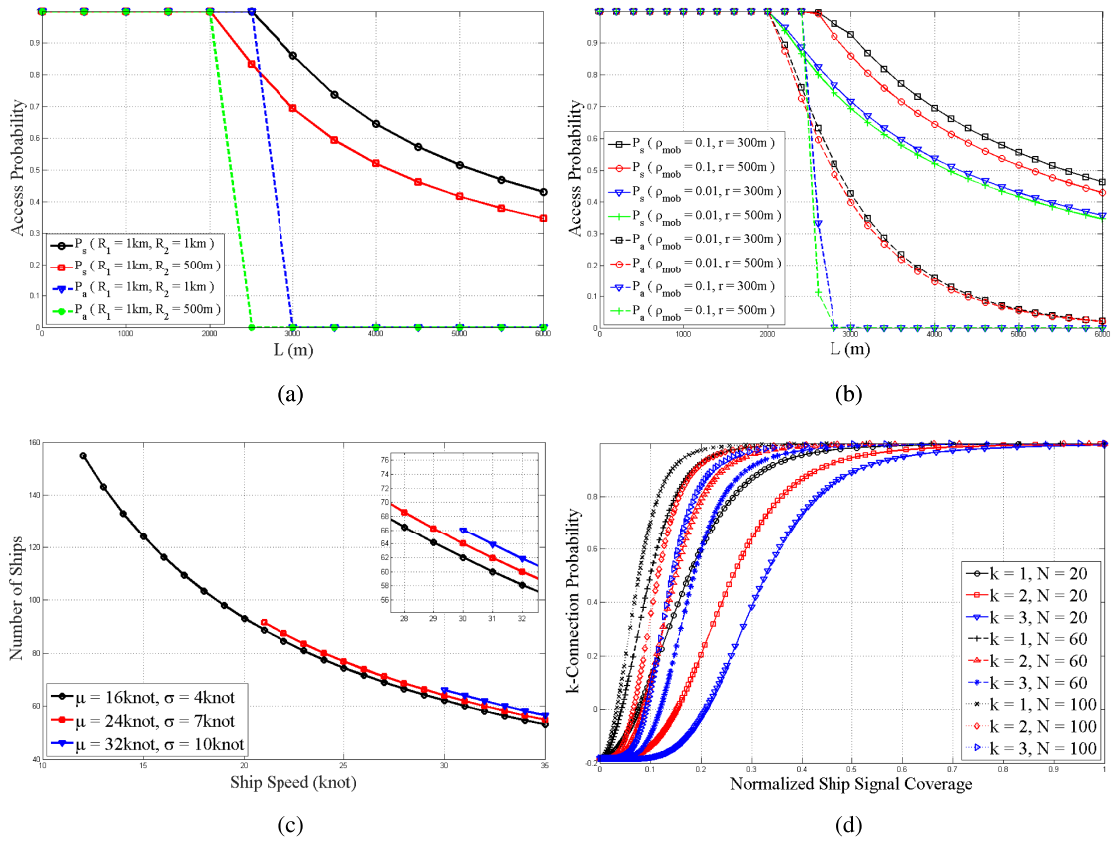

Fig. 9. Simulation results, where (a), (b), (c) are under the offshore network environment and (d) is under the open-sea network environment. (a) Access probability by varying the seacoast base station (SBS) coverage. (b) Access probability by varying mob and ship coverage. (c) Number of ships by varying the standard deviation of ship speed. (d) k-connection probability by varying the number of ships.

$1\,km$, respectively. The maximum neighbor SBSs distance is $8\,km$; the mean of ship speeds are fixed as $16knot$, $24knot$, and $32knot$, and each mean speed is with the standard deviation of ship speed $4knot$, $7knot$, and $10knot$, respectively. The simulation results are observed by varying the above parameters with analysis and discussion thereafter.

A. Under Offshore Network Environment

Fig. 9(a) shows the access probability of P_s and P_a with two SBSs employed. The SBS coverages (R_1 and R_2) are set to $500\,m$ and $1\,km$, respectively. In this simulation, we set $\rho_{mob} = 0.1$, and $r = 300\,m$. As shown in Fig. 9(a), the access probability decreases, as the SBS spacing L extends. This indicates that rationally replacing the SBS is crucial to maintaining a successful ship access rate. For example, when the SBS spacing is $3\,km$, not all ships can access SBS, and they need to multi-hop relay information to SBS. The access probability of a single ship connecting SBS, e.g., an access rate of approximately 0.65 for SBS spacing set to $4\,km$, is higher than all ship access rates. However, it decreases, as the SBS coverage is decreased.

Fig. 9(b) shows the access probability of P_s and P_a with two SBSs, and the coverage of each SBS is set to $1\,km$. In this simulation, the values of ρ_{mob} and r are varied. It is observed from Fig. 9(b) that the MN access probability is determined by the ship signal coverage and density. For example, when the SBS spacing is set to $4\,km$ and $\rho_{mob} = 0.1$, the access rate decreases by 6% if the ship coverage declines from $500\,m$ to $300\,m$. On the other hand, the access rate can decrease by approximately 17%, when the ship density turns to 0.01 and $r = 500\,m$. The ship access rate P_a in all cases shows a shape decrement, because the probability of any ship out of SBS connection dramatically declines as the ship density changed from 0.1 to 0.01 and the space of SBSs becomes larger.

It is observed from Fig. 9(c) that the number of ships decreases with an increase in the ship speed, thereby reflecting the navigation characteristics of ships in offshore marine networks. For the same standard deviation, the number of ships decreases, as the speed of the ship increases, indicating that the ship's flow affects the ship's density. In addition, the increase in standard deviation results in an increase in the number of ships and a corresponding increase in the connectivity of the network.

B. Under Open-Sea Network Environment

Fig. 9(d) shows the k-connection probability under the open-sea environment, where the simulated number of ships is varied between 20, 60, and 100. It is observed from Fig. 9(d) that the connection probability decreases, as the connection index k

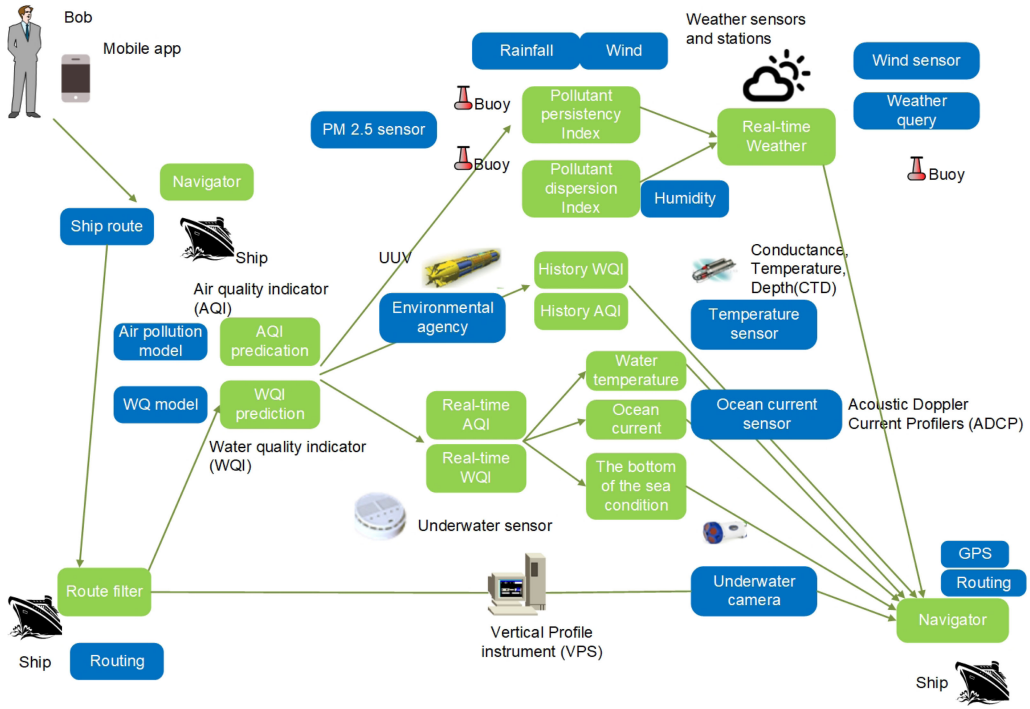

Fig. 10. Maritime edge services.

increases. For example, when 20 ships communicate with each other, 90% of them have at least one neighbor to connect as the normalized ship signal is 0.34. However, only half of them can have three connections simultaneously. The probability of ship connections increases with an increase in the number of ships joining MN with each ship associated with a larger signal coverage.

C. Maritime Edge Services And Computing Capability

Fig. 10 shows the representative maritime applications supported by edge services. For example, weather forecasts can be seamlessly shared to all interesting destinations, such as the personnel on ships or submarines. Another example is the maritime traffic data can be shared so that the routes for these vessels are optimally planned. A data platform may also be used for applications (like diving site searching) that are less critical than transportation control.

In order to analyze the maritime edge computing capacity, we assume that the maritime vehicles are with a certain amount of computing capability. The evaluation is conducted in the spatial domain within 170 $km * 500\ km$ offshore area of cities of Hong Kong and Shanghai. The information on maritime vehicles used for the simulation, such as ship ID, locations, and trajectories, is obtained via ten days observation on the AIS big data platform.

Fig. 11 illustrates the edge computing capacity along the seacoasts of cities of Hong Kong and Shanghai. The bright color represents a higher edge computing capability. The bright color portions are generated by counting the number of maritime vehicles over ten days. According to Fig. 11, we notice that the capacity at the offshore area is larger than the counterpart at the open-sea area because of more active ships near the coastline. This reflects that the computation capacity distribution is relevant to physiognomy, for example, a "Rive"-shape shows a strong computation area in Shanghai that is able to improve the edge services.

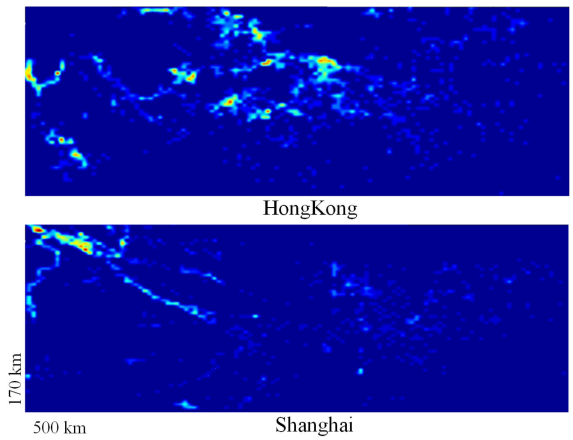

Fig. 11. Examples of edge computing capability.

VI. Conclusion

This work studies an MN networking method in terms of offshore and open-sea MN probabilistic connectivity. By analyzing and comparing the related works, we have simulated our models, and the simulation results have confirmed the validity of the proposed model. In addition, we have clarified the edge-based services of MN and analyzed the edge computation capability based on the cognitive big data platform. We expect that the research findings of this work can be valuable for the 5/6G MN

construction and implementation, as these findings provide a deep understanding of MN's connectivity characteristics and edge capabilities.

The future works will be committed to the deployment of the intelligent maritime infrastructure as mentioned in this paper. Another interesting direction to extend our study is to realize and optimize the maritime service platform and to improve the practicality and stability.

APPENDIX

Proof of Lemma-1:

Let K denote the set of ships directly connected to SBS_1 or SBS_2, where $K \in N$. The number of K ships, denoted as $card(K)$, demonstrates a probability of

$$\mathrm{P}\left(card(K)=i\right)=\sum_{i=j}^{\infty}\mathrm{P}\left(card(N)=j\right)* \mathrm{P}\left(card(K)=i|card(N)=j\right) \quad (73)$$

By combined such a probability with Equation (29), the probability of a ship belonging to K is defined by

$$q=\frac{1}{L}\int_0^L P_1(x)dx.$$

As the probabilities of a ship being directly connected to SBS_1 or SBS_2 are independent, the probability of the number of i ships in K belonging to the number of j ships in N follows the binomial distribution $B(j,q)$. By combining Equations (7), (24), and (25) along with the aforementioned conclusions, we obtain

$$P\left(card(K)=i\right)=\sum_{i=j}^{\infty}\frac{(\rho_{mob}L)^j}{j!}e^{-\rho L}\binom{j}{i}q^i(1-q)^{j-i}$$

$$=\left(\int_0^L\rho_{mob}p_1(x)dx\right)^i\frac{\exp\left(-\int_0^L\rho_{mob}p_1(x)dx\right)}{i!}.$$

In addition, when $[0, L]$ is divided into $\tilde{l}$ sections, the number of ships directly connected to at least one SBS in any section is expressed as $card(K(\tilde{l}))$. Thus we obtain

$$\mathrm{P}\left(card\left(K\left(\tilde{l}\right)\right)=i\right)=\left(\int_{x\in m}\rho_{mob}p_1(x)dx\right)^i* \frac{\exp\left(-\int_{x\in m}\rho_{mob}p_1(x)dx\right)}{i!}.$$

For the m mutually disjoint segments $\tilde{l_1}, \tilde{l_2}, \ldots, \tilde{l_m}$ in $[0, L]$, the random variables $card(K(\tilde{l_1}))...\, card(K(\tilde{l_m}))$ are independent of each other, as the ship directly connecting to SBS_1 or SBS_2 is not affected by others. Thus, the proof is completed.

Proof of Lemma-2:

Divide $[0, L]$ into $\frac{L}{dy}$ non-overlapping intervals by a very small value of dy; the probability of having multiple ships in dy is also small, the probability of one ship in dy is denoted as $\rho_{mob}dy$, and the probability of a ship in the segment of $[y, y+dy]$ belonging to K is denoted as $\rho_{mob}p_1(y)dy$. Moreover, the probability of ships with a distance of $|x-y|$ connecting to each other is $g_s(|x-y|)$. Therefore, the probability that the ship at x from SBS is directly connected to the ship in K located at $[y, y+dy]$ is $\rho_{mob}\cdot p_1(y)\cdot dy\cdot(g_s|x-y|)$. Let $I(x,y)$ denote the probability that a ship with a distance of x from SBS is not directly connected to any ship in K at $[0, y]$. As the pair-ship connections are independent, the ships at x that are not directly connected to any ships in K at interval $[0, y]$ are independent of the same ships not directly connected to ships in K at $[y, y+dy]$. The following formula is thus obtained:

$$I\left(x,y+dy\right)=I(x,y)\left(1-\rho_{mob}\cdot p_1(y)\cdot dy\cdot g_s\left(|x-y|\right)\right),$$

where the second term on the right side is a supplement to the probability that the ship at x is directly connected to the ship in K at an interval of $[y, y+dy]$. Therefore, the probability that the ship at x is not directly connected to any ship in K is obtained by integral transformation, and the proof is completed.

REFERENCES

[1] X. Su, B. Hui, and K. Chang, "Multi-hop clock synchronization based on robust reference node selection for ship ad-hoc network," *J. Commun. Netw.*, vol. 18, no. 1, pp. 65–74, 2016.

[2] S. W. Jo and W. S. Shim, "LTE-maritime: High-speed maritime wireless communication based on lte technology," *IEEE Access*, vol. 7, pp. 53 172–53 181, 2019.

[3] V. F. Arguedas, G. Pallotta, and M. Vespe, "Maritime traffic networks: From historical positioning data to unsupervised maritime traffic monitoring," *IEEE Trans. Intell. Transp. Syst.*, vol. 19, no. 3, pp. 722–732, Mar. 2017.

[4] X. Song and M. Yuan, "Performance analysis of one-way highway vehicular networks with dynamic multiplexing of eMBB and URLLC traffics," *IEEE Access*, vol. 7, pp. 118 020–118 029, 2019.

[5] P. Thulasiraman and K. A. White, "Topology control of tactical wireless sensor networks using energy efficient zone routing," *Digit. Commun. Netw.*, vol. 2, no. 1, pp. 1–14, 2016.

[6] A. Pughat and V. Sharma, "Performance analysis of an improved dynamic power management model in wireless sensor node," *Digit. Commun. Netw.*, vol. 3, no. 1, pp. 19–29, 2017.

[7] N. Hassan, K.-L. A. Yau, and C. Wu, "Edge computing in 5G: A review," *IEEE Access*, vol. 7, pp. 127 276–127 289, 2019.

[8] Y. Li, S. Xia, M. Zheng, B. Cao, and Q. Liu, "Lyapunov optimization based trade-off policy for mobile cloud offloading in heterogeneous wireless networks," *IEEE Trans. Cloud Comput.*, to be published, doi: 10.1109/TCC.2019.2938504.

[9] Y. Li, J. Liu, B. Cao, and C. Wang, "Joint optimization of radio and virtual machine resources with uncertain user demands in mobile cloud computing," *IEEE Trans. Multimedia*, vol. 20, no. 9, pp. 2427–2438, Sep. 2018.

[10] K.-L. A. Yau, A. R. Syed, W. Hashim, J. Qadir, C. Wu, and N. Hassan, "Maritime networking: Bringing internet to the sea," *IEEE Access*, vol. 7, pp. 48 236–48 255, 2019.

[11] Y. Ai, M. Peng, and K. Zhang, "Edge computing technologies for internet of things: A primer," *Digit. Commun.*, vol. 4, no. 2, pp. 77–86, 2018.

[12] A. Anand and G. de Veciana, "Resource allocation and harq optimization for URLLC traffic in 5G wireless networks," *IEEE J. Sel. Areas Commun.*, vol. 36, no. 11, pp. 2411–2421, Nov. 2018.

[13] F. Tang, Y. Kawamoto, N. Kato, and J. Liu, "Future intelligent and secure vehicular network toward 6G: Machine-learning approaches," *Proc. IEEE*, vol. 108, no. 2, pp. 292–307, Feb. 2020.

[14] J. Kang, O. Simeone, and J. Kang, "On the trade-off between computational load and reliability for network function virtualization," *IEEE Commun. Lett.*, vol. 21, no. 8, pp. 1767–1770, Aug. 2017.

[15] K. Alhazmi, A. Shami, and A. Refaey, "Optimized provisioning of sdn-enabled virtual networks in geo-distributed cloud computing datacenters," *J. Commun. Netw.*, vol. 19, no. 4, pp. 402–415, 2017.

[16] J. Ren, H. Guo, C. Xu, and Y. Zhang, "Serving at the edge: A scalable iot architecture based on transparent computing," *IEEE Netw.*, vol. 31, no. 5, pp. 96–105, Aug. 2017.

[17] W. Zhang *et al.*, "Multi-hop connectivity probability in infrastructure-based vehicular networks," *IEEE J. Sel. Areas Commun.*, vol. 30, no. 4, pp. 740–747, May 2012.

[18] Y. Huang, B. Hui, X. Su, and K. Chang, "Self-weighted decentralized cooperative spectrum sensing based on notification for hidden primary user detection in sanet-cr network," *KSII Trans. Internet Inf. Syst.*, vol. 7, no. 11, 2013.
[19] X. Su, H.F. Yu, K.H. Chang, S.-G. Kim, and Y.-K. Lim, "Case study for ship ad-hoc networks under a maritime channel model in coastline areas." *KSII Trans. Internet & Inform. Syst.*, vol. 9, no. 10, pp. 4002–4014, Oct. 2015.
[20] F. Papi *et al.*, "Radiolocation and tracking of automatic identification system signals for maritime situational awareness," *IET Radar, Sonar Navigation*, vol. 9, no. 5, pp. 568–580, 2014.
[21] H. Zhang, Q. Huang, F. Li, and J. Zhu, "A network security situation prediction model based on wavelet neural network with optimized parameters," *Digit. Commun. Netw.*, vol. 2, no. 3, pp. 139–144, 2016.
[22] B. Hui, K. Jeon, K. Chang, S. Kim, J. Park, and Y. Lim, "Design of radio transmission technologies for VHF band ship ad-hoc network," in *Proc. Int. Conf. ICT Convergence*, 2011, pp. 626–629.
[23] X. Su, B. Hui, K. Chang, and G. Jin, "Case study of 3GPP LTE and IEEE 802.11 p systems for ship ad-hoc network," in *Proc. 18th Asia-Pacific Conf. Commun.*, 2012, pp. 546–547.
[24] X. Su, B. Hui, K. Chang, and S. Kim, "Improvement of the link reliability for ship ad-hoc network by employing multiple antennas," *Korea Inf. Commun. Soc.*, vol. 37, no. 12, pp. 1065–1075, 2012.
[25] P. K. Sahoo, M.-J. Chiang, and S.-L. Wu, "Connectivity modeling of vehicular ad hoc networks in signalized city roads," in *Proc. 40th Int. Conf. Parallel Process. Workshops*, 2011, pp. 22–26.
[26] X. Hou, Y. Li, M. Chen, D. Wu, D. Jin, and S. Chen, "Vehicular fog computing: A viewpoint of vehicles as the infrastructures," *IEEE Trans. Veh. Technol.*, vol. 65, no. 6, pp. 3860–3873, Jun. 2016.
[27] S. Kwon, Y. Kim, and N. B. Shroff, "Analysis of connectivity and capacity in 1-D vehicle-to-vehicle networks," *IEEE Trans. Wireless Commun.*, vol. 15, no. 12, pp. 8182–8194, Dec. 2016.
[28] J. Wu, "Connectivity analysis of a mobile vehicular ad hoc network with dynamic node population," in *Proc. IEEE Globecom Workshops*, 2008, pp. 1–8.
[29] S. C. Ng, W. Zhang, Y. Zhang, Y. Yang, and G. Mao, "Analysis of access and connectivity probabilities in vehicular relay networks," *IEEE J. Sel. Areas Commun.*, vol. 29, no. 1, pp. 140–150, Jan. 2010.
[30] J. Zhao, Y. Chen, and Y. Gong, "Study of connectivity probability of vehicle-to-vehicle and vehicle-to-infrastructure communication systems," in *Proc. IEEE 83rd Veh. Technol. Conf.*, 2016, pp. 1–4.
[31] C. Li, A. Zhen, J. Sun, M. Zhang, and X. Hu, "Analysis of connectivity probability in vanets considering minimum safety distance," in *Proc. 8th Int. Conf. Wireless Commun. Signal Process.*, 2016, pp. 1–5.
[32] B. Pan and H. Wu, "Performance analysis of connectivity considering user behavior in V2V and V2I communication systems," in *Proc. IEEE 86th Veh. Technol. Conf.*, 2017, pp. 1–5.

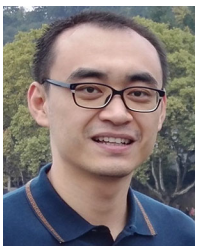

Xin Su (Senior Member, IEEE) received the B.E. degree in computer engineering from the Kunming University of Science and Technology, China, in 2008, and the M.E. degree in computer engineering from Chosun University, South Korea, in 2010, and the Ph.D. degree from the Program in IT & Media Convergence Studies, Inha University, South Korea, in 2015.

He currently is an Associate Professor at the College of IoT Engineering, Hohai University, China. He recently focuses the research topics on mobile communication, 5/6G systems, edge computing/fog computing, IoT applications, and smart ocean. Recent years, he has published more than 70 academic papers, including IEEE TRANSACTIONS ON INDUSTRIAL. INFORMATICS, *Future Generation Computer System*, IEEE TRANSACTIONS ON SUSTAINABLE COMPUTING, *IEEE Consumer Electronics Magazine, MONET* and so on. Dr. Su currently works on the editorial board of *Digital Communications & Networks*, and has served as the organizer of International Conferences, including IEEE CCNC, IEEE ISPA, ACM RACS, ACM SAC, and I-SPAN.

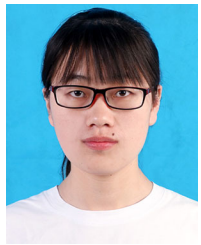

Leilei Meng received the B.E. degree in communication and information systems from the College of IOT Engineering, Hohai University, China, in 2020. She is currently a member of the Lab of Network & Communication supervised by Dr. Xin Su, and pursuing her M.S. degree at Hohai University. Her research interests include mobile communication, 5/6G systems, and maritime networks.

Jun Huang (Senior Member, IEEE) received the Ph.D. degree (with honor) from the Institute of Network Technology, Beijing University of Posts and Telecommunications, China, in 2012. He is a Full Professor of computer science with the Chongqing University of Posts and Telecommunications.

Dr. Huang was a Visiting Scholar in the Global Information and Telecommunication Institute, Waseda University, a Research Fellow in the Electrical and Computer Engineering Department, South Dakota School of Mines and Technology, a Visiting Scholar in the Computer Science Department, the University of Texas at Dallas, and a Guest Professor at the National Institute of Standards and Technology. He received the Outstanding Service Award from ACM RACS 2017, 2018, and 2019, the runner-up of Best Paper Award from ACM SAC 2014, and the Best Paper Award from AsiaFI 2011. He has authored 120+ publications including papers in prestigious journal/conferences such as the IEEE TRANSACTIONS ON WIRELESS COMMUNICATIONS, THE IEEE NETWORK, THE IEEE COMMUNICATIONS MAGAZINE, THE IEEE WIRELESS COMMUNICATIONS, THE IEEE TRANSACTIONS ON BROADCASTING, THE IEEE TRANSACTIONS ON VEHICULAR TECHNOLOGY, THE IEEE TRANSACTIONS ON EMERGING TOPICS IN COMPUTING, THE IEEE TRANSACTIONS ON NETWORK AND SERVICE MANAGEMENT, THE IEEE TRANSACTIONS ON SUSTAINABLE COMPUTING, THE IEEE INTERNET OF THINGS JOURNAL, THE IEEE TRANSACTIONS ON CLOUD COMPUTING, THE IEEE TRANSACTIONS ON COGNITIVE COMMUNICATIONS AND NETWORKING, IEEE/ACM INTERNATIONAL SYMPOSIUM ON QUALITY OF SERVICE, SCC, INTERNATIONAL CONFERENCE ON COMPUTER COMMUNICATIONS AND NETWORKS, IEEE GLOBAL COMMUNICATIONS CONFERENCE, ICC, ACM SYMPOSIUM ON APPLIED COMPUTING, and RACS. He is an Associate Editor of IEEE ACCESS and the *KSII Transactions on Internet and Information Systems*. He guest-edited several special issues on IEEE journals such as the IEEE COMMUNICATIONS MAGAZINE, the IEEE INTERNET OF THINGS JOURNAL, the IEEE ACCESS, etc. He also chaired and co-chaired multiple conferences in the communications and networking areas and organized multiple workshops at major IEEE and ACM events. His current research interests include network optimization and control, machine-to-machine communication, and the Internet of Things.